

Experimental quantification of the hysteretic and vibration damping of dry-joint masonry structures

Colombo Carla ^a, Vlachakis Georgios ^{a*}, Savalle Nathanaël ^b,
Giouvanidis Anastasios I. ^c, Lourenço Paulo B. ^a

^a University of Minho, ISISE, ARISE, Department of Civil Engineering, 4800-058 Guimarães, Portugal

^b Université Clermont Auvergne, Clermont Auvergne INP, CNRS, Institut Pascal F-63000 Clermont-Ferrand, France

^c Department of Civil and Environmental Engineering, University of Auckland, Auckland, New Zealand

*Corresponding author: giorgovlachaki@gmail.com

Abstract

A variety of heritage structures worldwide are constructed using dry-joint masonry blocks. The structural integrity of such structures strongly relies on the mechanical properties of the contact interface between the blocks, which include the frictional properties, the interface stiffness and the interface damping. Among them, the interface damping has attracted less attention in the scientific literature, while it plays an essential role in the global response of these assemblies when subjected to earthquakes. To this end, this paper presents a thorough experimental characterisation campaign on dry-joint limestone blocks focusing on the interface damping. More specifically, two distinct types of energy dissipation are identified and characterised using an equivalent viscous damping representation: (i) the hysteretic and (ii) the vibration damping. In this work, the hysteretic energy losses are experimentally quantified after joint closure tests, and the vibration damping is measured through ambient vibration tests on dry-joint assemblies. The results show different damping ratios for the various types of damping and a rather constant response with respect to normal stress at the interface.

Keywords: contact mechanics; dry-joint; interface damping; masonry structures; viscous damping

Introduction

A significant portion of heritage structures, such as the Egyptian pyramids, the classical Greek temples, the Roman aqueducts, the Inca's citadels and many Indian temples, among others, are constructed using dry-joint masonry blocks. The structural integrity and failure of such structures are mainly dictated by the dry-joint contact interfaces rather than the blocks themselves [1]. Therefore, it is of paramount importance to describe the mechanical behaviour of these interfaces, to have a more accurate assessment of such structures. The main mechanical properties of the interfaces include the frictional properties [2, 3], the interface stiffness [3, 4] and the interface damping [5]. Among them, the interface damping has attracted less attention in the scientific literature, while it plays an essential role in the energy dissipation of these assemblies when subjected to dynamic actions, such as earthquakes.

The mechanical interpretation, quantification and description of the interface damping are issues of exceptional difficulties [6]. Specifically, the contact mechanics resort to different scales depending on the engineering field, commonly at the micro (in the order of 10^{-6} m), meso (in the order of 10^{-2} m) or macro (in the order of 10^2 m) scales. Heritage masonry structures, in particular, span over the meso and macro scale, where the description of the interface damping adopts various phenomenological models. Recent developments in computational mechanics of numerical block-based models (e.g. the finite or discrete element methods [7]) have drawn significant attention at the meso scale [8]. Nevertheless, researchers tend to adopt values and models of the interface damping on an empirical basis or after a posteriori fitting to an experimental response of much higher complexity [8, 9]. Therefore, it becomes clear that experimental studies on the characterisation of the interface damping are of paramount importance in order to describe the energy losses of dry-joint masonry structures.

To this end, this paper presents an experimental characterisation campaign of the interface damping of dry-joint limestone blocks. Two types of damping are identified and quantified using an equivalent viscous damping representation: (i) the hysteretic and (ii) the vibration damping. The hysteretic damping is observed and quantified after joint-closure cyclic tests, while the vibration damping is measured through ambient

vibration tests on dry-joint assemblies. The outcomes of the experimental campaign provide a quantification of the energy losses of dry-joints, with the aim of a more accurate assessment of dry-joint masonry heritage structures.

Experimental Campaign

The experimental campaign focuses on the interfaces of hard limestone specimens. At the meso-scale, the specimens' surfaces appear heterogeneous with the presence of distributed shell segments and fossil debris. Moreover, the bulk properties of the limestone are initially characterised, and found to have density of $\rho = 2238 \text{ kg/m}^3$, compressive strength $f_c = 47.6 \text{ MPa}$ and elastic modulus of $E_{stone} = 32.7 \text{ GPa}$ [5].

The hysteretic damping is quantified using 20 quasi-static joint-closure cyclic tests. 10 cylindrical specimens with 64.7 mm diameter and 80.5 mm height are extracted from bigger limestone blocks (Fig. 1a), while the dry-joint interfaces among the different specimens are kept intact from the original ones. Then, the cylinders are placed on top of each other and compressed with an actuator, as shown schematically in Fig. 1b. Moreover, three Linear Variable Differential Transformers (LVDTs) are mounted around the specimens to measure the joint displacement, while a load cell within the actuator measures the applied normal load. Clearly, the LVDT's measurements include both the bulk deformability and the joint closure $u_{j,n}$, and thus the latter can be extracted as:

$$u_{j,n} = u_{LVDT} - \frac{\sigma_n \cdot L_{LVDT}}{E_{stone}} \quad (1)$$

where u_{LVDT} is the acquired measurement from the LVDT, σ_n is the applied normal stress at the interface and L_{LVDT} is the specimen's height monitored by the LVDTs, shown in Fig. 1b. Fig. 1c illustrates the response of a representative joint-closure test, displaying a notable non-linear behaviour. More specifically, the interface is characterised by gradual stiffening, hysteresis upon unloading and further hysteresis for consecutive reloading. Fig. 1d-e indicates the associated dissipated energy E_d upon unloading (Fig. 1d) and reloading (Fig. 1e), together with the elastic stored energy at maximum response E_e , for one representative cycle. Assuming a unilateral viscous dashpot representation, then the damping ratio ξ_{hyst} that satisfies energy loss equivalence is [11]:

$$\xi_{hyst} = \frac{1}{2\pi} \cdot \frac{E_d}{E_e} \quad (2)$$

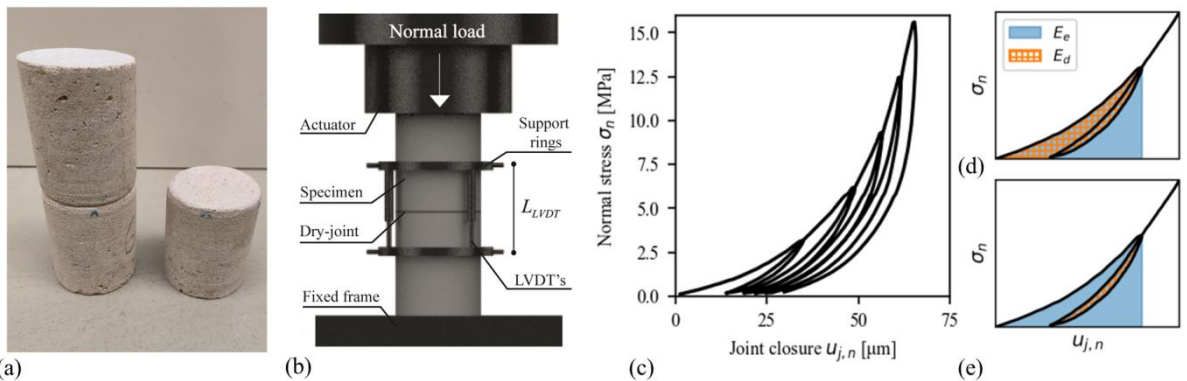


Fig. 1 Joint-closure tests: (a) adopted cylindrical specimens, (b) scheme of experimental setup, (c) representative joint-closure response, and stored E_e and dissipated E_d energies for representative (d) unloading cycle, and (e) reloading cycle.

The vibration interface damping is estimated by measuring the dynamic properties of a dry-joint assembly. More specifically, one squared specimen is placed on the ground (base block) and another one (top block) is placed on top of the former, thus forming the interface under investigation. The base block has dimensions

270×720×90 mm (width, length, height), while various top blocks are employed to examine the interface-to-interface variability, with 50×150 mm base dimensions (width, length) and various heights ranging from 200 to 750 mm. Moreover, with the aim of examining the interface damping properties for even higher normal stresses at the interface, some tests are conducted with additional steel weights, glued on top of the top block. The examined specimens are excited by the ambient noise of the laboratory, and thus the specimens experience vibrations of very low amplitude (perturbations), which permits the use of linear dynamics. Three accelerometers are placed at the top block and one at the base block to measure the vibrations of the specimens. Afterwards, the acquired signals are post-processed using the Enhanced Frequency Domain Decomposition (EFDD) method [12, 13] to estimate the damping ratio of the interfaces, shown in Fig. 2. In brief, the EFDD transforms the acquired accelerations in the frequency domain using the Welch's method of the Fast Fourier Transformation (FFT) and constructs the cross Power Spectral Density (PSD) matrix. Subsequently, the Singular Value Decomposition (SVD) is applied on the cross PSD, which represents Equivalent Single Degree Of Freedom systems, with their mode shapes given by the singular vectors. Importantly, the mode shapes allow the identification of the modes of vibration that are associated with the perturbations of the interfaces. In particular, three mode shapes related to the interfaces are identified, corresponding to the two rotations of the top block over the two horizontal axes (mode XX and YY) and the rotation of the top block over the vertical axis (mode ZZ). After the identification of the interface modes using peak picking, the spectral regions that retain a coherent mode shape are isolated using the Modal Assurance Criterion (MAC), commonly referred to as ESDOF "bells". These "bells" represent auto-correlation functions of the ESDOF when transformed back to the time domain using the Inverse Fast Fourier Transformation (IFFT). Finally, the vibration damping ratio ξ_{vibr} of each identified ESDOF is computed in the time domain using the logarithmic decrement method. It is worth underlying that, to avoid biased results, the autocorrelation is divided by a triangular window, for which amplitudes larger than 0.85 and lower than 0.25 are disregarded during the damping estimation procedure [13]. Moreover, the estimation of the vibration damping using the EFDD is also affected by the time segments' length used in the Welch's method [14]. To achieve a reliable estimation of the damping ratio, the present study adopts a convergence analysis strategy during which each test is iteratively analysed by increasing the time segment length until convergence of the damping ratio is achieved [5].

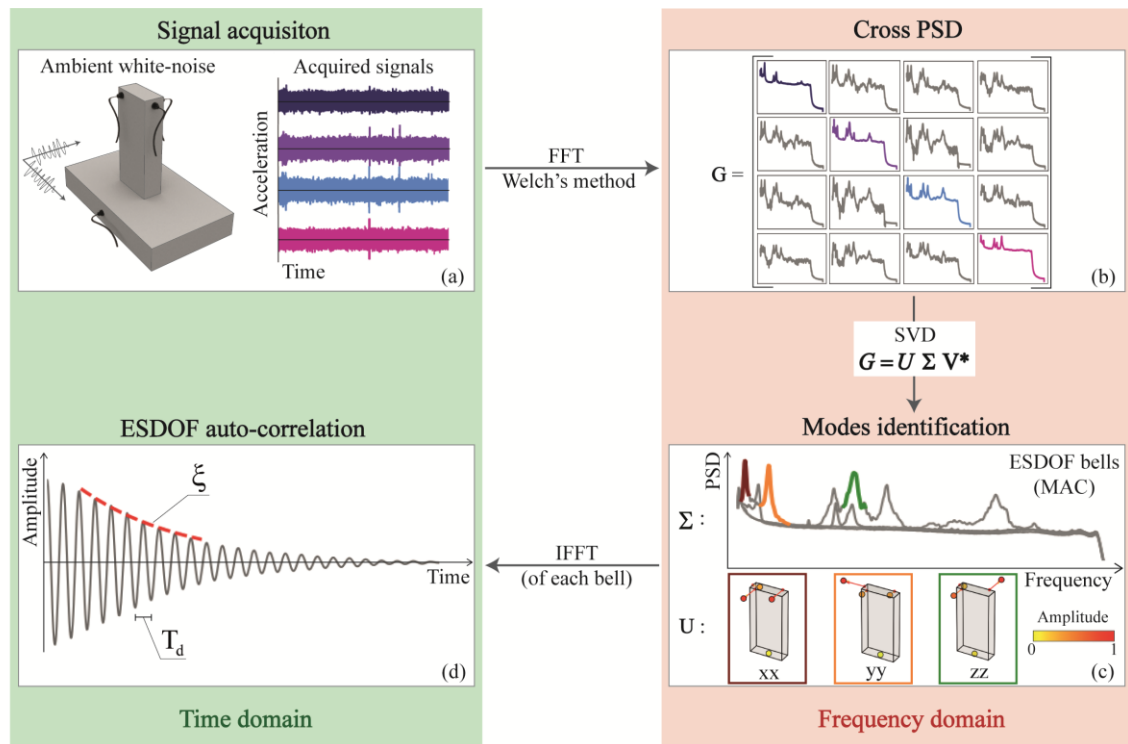


Fig. 2 Dynamic identification tests and workflow of the Enhanced Frequency Domain Decomposition (EFDD) method: (a) signal acquisition under ambient white noise excitation, (b) cross Power Spectral Density (PSD) matrix using the Welch's method, (c) Singular Value Decomposition (SVD) of cross PSD and modes identification (frequencies and mode shapes), and (d) autocorrelation of identified Equivalent Single Degree Of Freedom (ESDOF) modes using Inverse Fast Fourier Transformation (IFFT).

Interface Damping

The interface damping outcomes of the experimental campaign are shown in Fig. 3. More specifically, Fig. 3a illustrates the hysteretic interface damping ratio, measured after the joint-closure tests. The tests showed hysteresis upon unloading (Fig. 1d) and upon consecutive reloading (Fig. 1e). The former are related to the plastic deformation of the protruding asperities and the friction phenomena between the partially oblique asperities at the micro scale upon joint closure/opening [15], thus denoted as ξ_{pl+fr} , while the latter are associated only with the friction phenomena of the oblique asperities, thus denoted as ξ_{fr} . Fig. 3a quantifies both hysteretic damping ratios against the applied normal stress σ_n . In more detail, the ξ_{pl+fr} ranges between 7 and 12 %, with a median value of 9.2 %, while it also shows an increasing trend for higher values of applied normal stress. On the other hand, the ξ_{fr} ranges from 1.5 to 3 %, with a median value of 2% and a rather constant value for different normal stress levels.

The vibration damping ratio is depicted in Fig. 3b, following the ambient vibration tests and the use of the EFDD post-processing methodology (Fig. 2). Three groups are distinguished based on the vibrational modes, i.e. modes XX, YY and ZZ. Similar to the hysteretic damping, the results are plotted against the applied normal stress σ_n at the examined interface, although herein of a much lower order of magnitude since it stems only from the self-weight of the specimens. Overall, the vibration damping presents values between 0.15 and 5 %, with the median value of around 1 %. The results are practically constant and do not show any strong dependency on the applied normal stress σ_n , yet higher normal stresses reduce the scatter of the outcomes. Moreover, small differences are observed among the different modes of vibration, with the XX, YY and ZZ having median values of 1.28%, 1.01% and 0.75%, respectively. Nevertheless, the vibration damping of mode XX shows higher scatter than that of mode YY, followed by the less scattered results of mode ZZ.

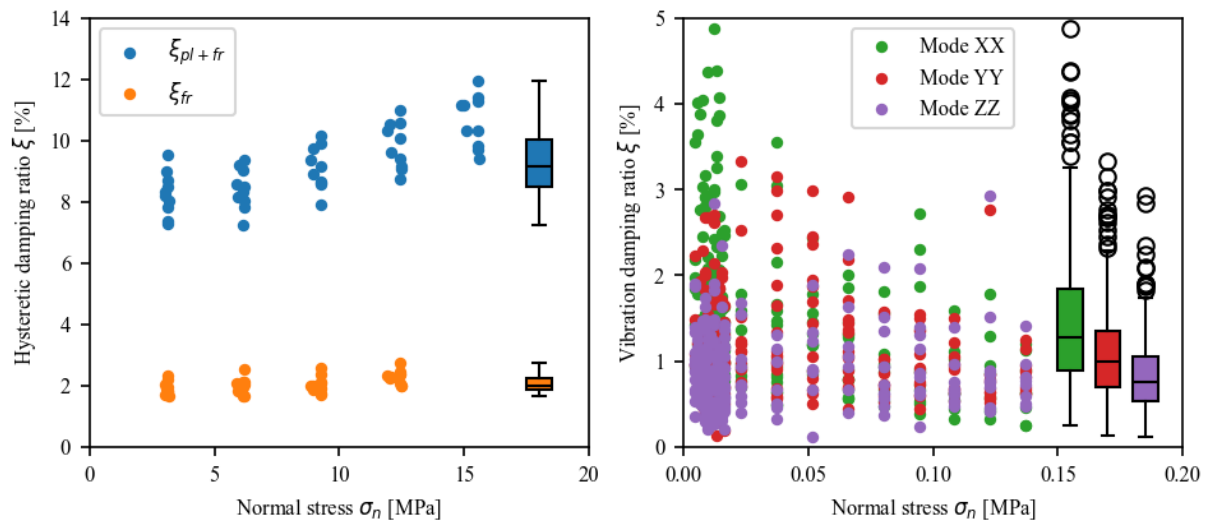


Fig. 3 (a) Hysteretic and (b) vibration damping ratios ξ with respect to normal stress σ_n at the interface.

Conclusions

This work presents an extensive experimental campaign for the characterisation of the interface damping of dry-joint masonry assemblies. To this end, two different experimental setups are employed and two distinct types of interface damping are quantified: i) the hysteretic damping after joint-closure tests, and ii) the vibration damping following dynamic identification tests. Both types of interface damping are important as they describe different underline physical phenomena of energy dissipation at the interface. The former is of static nature and arises due to the relative displacements at the interface, while the latter is inherently dynamic and occurs under vibration perturbations. More specifically, the results of the hysteretic damping are associated with plastic deformations and friction phenomena of oblique asperities at the micro scale and

show increasing damping ratios for higher normal stresses. On the other hand, the vibration damping indicates constant damping ratios, comparable dissipation for three identified modes of vibration (i.e. XX, YY and ZZ) and a reduced scatter for higher normal stresses at the interface. Overall, such a plethora of collected experimental data paves the way for the formulation of reliable constitutive laws of dry-joint interfaces.

References

- [1] C. Colombo, N. Savalle, A. Mehrotra, M. F. Funari, and P. B. Lourenço, “Experimental, numerical and analytical investigations of masonry corners: Influence of the horizontal pseudo-static load orientation,” *Constr. Build. Mater.*, vol. 344, 2022.
- [2] C. Colombo *et al.*, “Tangential Interface Stiffness Estimation of Dry-Joint Masonry Structures Through an Extended Experimental Campaign,” in *14th North American Masonry Conference*, 2023.
- [3] P. M. Naik, T. Bhowmik, and A. Menon, “Estimating joint stiffness and friction parameters for dry stone masonry constructions,” *Int. J. Mason. Res. Innov.*, vol. 6, no. 2, pp. 232–254, 2021.
- [4] C. Colombo *et al.*, “A Comparative Experimental Campaign to Estimate the Normal Interface Stiffness of Dry-Joint Masonry Structures,” *RILEM Bookseries*, vol. 41, pp. 213–223, 2023.
- [5] G. Vlachakis, C. Colombo, A. I. Giouvanidis, N. Savalle, and P. B. Lourenço, “Experimental characterisation of dry-joint masonry structures: Interface stiffness and interface damping,” *Constr. Build. Mater.*, vol. 392, 2023.
- [6] A. I. Vakis *et al.*, “Tribology International Modeling and simulation in tribology across scales : An overview,” *Tribol. Int.*, vol. 125, pp. 169–199, 2018.
- [7] A. M. D’Altri *et al.*, “Modeling Strategies for the Computational Analysis of Unreinforced Masonry Structures: Review and Classification,” *Arch. Comput. Methods Eng.*, vol. 27, pp. 1153–1185, 2019.
- [8] D. Malomo and B. Pulatsu, “Discontinuum models for the structural and seismic assessment of unreinforced masonry structures: a critical appraisal,” *Structures*, vol. 62, no. March, p. 106108, 2024.
- [9] G. Vlachakis, A. I. Giouvanidis, A. Mehrotra, and P. B. Lourenço, “Numerical block-based simulation of rocking structures using a novel universal viscous damping model,” *J. Eng. Mech.*, vol. 147, no. 11, p. 04021089, 2021.
- [10] D. Malomo, A. Mehrotra, and M. J. Dejong, “Distinct element modeling of the dynamic response of a rocking podium tested on a shake table,” *Earthq. Eng. Struct. Dyn.*, vol. 50, no. 5, pp. 1469–1475, 2021.
- [11] L. Jacobsen, “Damping in composite structures,” in *Proceedings of 2nd world conference on Earthquake Engineering*, 1960, pp. 1029–1045.
- [12] R. Brincker, C. E. Ventura, and P. Andersen, “Damping Estimation by Frequency Domain Decomposition,” in *Proceedings of IMAC 19*, 2001.
- [13] R. Brincker and C. E. Ventura, *Introduction to Operational Modal Analysis*. 2015.
- [14] F. Magalhães, Á. Cunha, E. Caetano, and R. Brincker, “Damping estimation using free decays and ambient vibration tests,” *Mech. Syst. Signal Process.*, vol. 24, no. 5, pp. 1274–1290, 2010.
- [15] C. H. Scholz and S. H. Hickman, “Hysteresis in the Closure of a Nominally Flat Crack,” *J. Geophys. Res. Solid Earth*, vol. 88, no. B8, pp. 6501–6504, 1983.